Nano Res. 2011, 4(2): 216–225
DOI 10.1007/s12274-010-0072-y
Research Article
ISSN 1998-0124
CN 11-5974/O4

Hierarchical Manganese Oxide/Carbon Nanocomposites for Supercapacitor Electrodes

Yiting Peng[1,2,§], Zheng Chen[2,§], Jing Wen[2], Qiangfeng Xiao[2], Ding Weng[2], Shiyu He[1] (✉), Hongbin Geng[1] (✉), and Yunfeng Lu[2] (✉)

[1] Department of Materials Science and Engineering, Harbin Institute of Technology, Harbin, 150001, China
[2] Department of Chemical and Biomolecular Engineering, University of California, Los Angeles, CA 90095, USA

Received: 14 October 2010 / Revised: 5 November 2010 / Accepted: 6 November 2010

ABSTRACT

MnO_2/carbon nanocomposites with hierarchical pore structure and controllable MnO_2 loading have been synthesized using a self-limiting growth method. This was achieved by the redox reactions of $KMnO_4$ with sacrificed carbon substrates that contain hierarchical pores. The unique pore structure allows the synthesis of nanocomposites with tunable MnO_2 loading up to 83 wt.%. The specific capacitance of the nanocomposites increased with the MnO_2 loading; the conductivity measured by electrochemical impedance spectroscopy, on the other hand, decreased with increasing MnO_2 loading. Optimization of the MnO_2 loading resulted in nanocomposites with high specific capacitance and excellent rate capability. This work provides important fundamental understanding which will facilitate the design and fabrication of high-performance supercapacitor materials for a large variety of applications.

KEYWORDS

Hierarchically porous carbon, MnO_2/carbon nanocomposite, supercapacitor

1. Introduction

Supercapacitors are emerging as a class of high-power energy-storage devices [1–4]; their broader uses, however, are still limited by their energy density [5–7]. Generally, a supercapacitor is based on the electrical double layers formed along carbon electrodes, which may provide capacitance of up to 300 F/g in an aqueous electrolyte [8, 9]. Oxides of transition metals, such as RuO_2 [10–12], MnO_2 [13–16], NiO [17, 18], Co_3O_4 [19], and V_2O_5 [20, 21], possess significantly higher capacitances; however, harvesting such capacitance has been limited by their low conductivity and redox kinetics. To address such intrinsic limitations, a common strategy is to integrate low-dimensional oxide materials with conductive components, such as carbon, which has led to the development of various nanocomposites with significantly improved energy density [22–24]. Nevertheless, many essential questions about such composites, such as how the structure, composition and interfaces of the composites may affect the capacitive performance, remain open.

We report herein the synthesis of MnO_2/carbon nanocomposites with controlled structure and composition and the study of the role of these properties in determining capacitive performance. MnO_2 is currently

§ These authors contributed equally.
Address correspondence to Shiyu He, syhe@21cn.com; Hongbin Geng, genghb@yahoo.com; Yunfeng Lu, luucla@ucla.edu

considered as one of the most promising redox components for supercapacitor applications owning to its high capacitance, low cost, and low toxicity. To date, various MnO_2/carbon composites have been synthesized, such as composites with planar graphite [25], acetylene black [26, 27], ordered mesoporous carbon [28, 29], carbon nanotubes [30–33], and carbon aerogels and nanofoams [34]. These have generally been synthesized by physical mixing of MnO_2 with carbon [31], or electrochemically or chemically depositing MnO_2 on carbon substrates [32, 33]. Among these synthesis methods, the chemical deposition of MnO_2 through self-limiting redox reactions of $KMnO_4$ and carbon is of particular interest [25–29]. In such a synthesis, carbon substrates are exposed to $KMnO_4$ solution at room temperature or an elevated temperature, and a spontaneous redox reaction described as

$$4MnO_4^- + 3C + 2H_2O \longrightarrow 4MnO_2 + 3CO_2 + 4OH^- \quad (1)$$

occurs producing MnO_2 on the sacrificial carbon substrates [35]. The resulting MnO_2 layer reduces the diffusion of the MnO_4^- ions, generating conformal MnO_2 coatings on the conductive carbon substrates. Such a self-limiting growth confers several major advantages, such as intimate interfaces between the oxide and the carbon, nanosized oxide particles, and controllable oxide thickness.

Nevertheless, the structure and composition of such MnO_2/carbon composites are governed by transport of the $KMnO_4$ in solution and its reaction with carbon, which is very rapid even at room temperature. Note that the diffusion of $KMnO_4$ in porous carbon substrates, such as activated carbon and mesoporous carbons, is generally slow in comparison with the fast reaction kinetics [36, 37]. The rapid reactions result in the preferential formation of MnO_2 layers located on the exterior of the carbon substrates, blocking inwards diffusion and reaction of $KMnO_4$. This technical difficulty inevitably leads to a low MnO_2 loading in the composites, which is detrimental for overall capacitance. Moreover, the formation of MnO_2 is often associated with reduced pore accessibility and electron conductivity. In fact, it has been observed that increasing the oxide loading in such carbon composites by further promoting the redox reaction resulted in a reduction in the overall capacitance [38]. Therefore, the synthesis of MnO_2/carbon composites with higher oxide loading and controlled pore structure for fast transport of ions, which retain the carbon framework needed for electron conductivity is essential to ensure a satisfactory capacitance performance.

To address this challenge, carbon substrates with hierarchical pores (pores with multiple-length-scale diameters) rather than uniform pores were used in this work. The presence of large pores ensures the effective transport of $KMnO_4$ to the substrate interior, while the mesopores provide high surface area for effective reaction. Such a structure allows the formation of composites with high oxide loadings that are homogenously and intimately coated on the sacrificial carbon scaffold. Moreover, the resulting nanocomposites still retain an interconnected porous structure, which facilitates effective electrolyte diffusion and charge transport and ensures higher specific capacitance and better rate capability. Resulting from this unique design, nanocomposites with MnO_2 loadings of up to 80 wt.% have been achieved, which is a significant advance on the current state of the art. For the first time, electrochemical impedance spectroscopy has been used to study the synergic effects between the MnO_2 mass loading and conductive carbon scaffold, providing insights leading to better capacitance performance.

2. Experimental

2.1 Synthesis of carbon substrate and MnO_2/carbon nanocomposites

The porous carbon substrates were synthesized by an assembly process using phenolic resol as the carbon precursor. Tri-block copolymer F127 (Mw = 12,600, $PEO_{106}PPO_{70}PEO_{106}$, where PEO and PPO are poly(ethylene oxide) and poly(propylene oxide), respectively) was used as a soft template; silicate clusters formed by hydrolysis and condensation reactions of tetraethyl orthosilicate (TEOS) and colloidal silica particles (70–100 nm in diameter) were used as the hard template. Briefly, F127 (1.6 g), 0.2 mol/L HCl (1.0 g), ethanol (8 g), TEOS (2.08 g), and colloidal silica (1.5 g) were mixed in a flask and vigorously stirred

for 4 h. The mixture was transferred to a glass dish and after evaporation of the solvent for 12 h at room temperature, the mixture was put into an oven at 100 ℃ for 24 h to effect the thermo-polymerization. The samples were then carbonized in a tubular furnace under nitrogen flow. The samples were heated from room temperature to 350 ℃ at 2 ℃/min, kept at 350 ℃ for 2 h and heated to 500 ℃ at 1 ℃/min, followed by heating to 900 ℃ at 10 ℃/min and holding at 900 ℃ for 2 h. After carbonization, the as-formed carbon/silica composites were soaked with 5 wt.% HF for 12 h to remove the silica, converting the composites into hierarchical porous carbons. For comparison, ordered mesoporous carbon (OMC) with a uniform pore structure was also synthesized according to the method reported by Zhao et al. [39].

The synthesis of MnO_2/carbon composites was conducted by a procedure adapted from the Ref. [25]. Briefly, 0.08 g of carbon substrate was soaked in 25 mL of Na_2SO_4 solution (0.1 mol/L) at 50 ℃ in vacuum and stirred with 25 mL solution containing 0.1 mol/L $KMnO_4$ and 0.1 mol/L Na_2SO_4 for 1, 5, 10, 30, 60, 120, or 240 min. The products were then washed with deionized water and dried at 80 ℃ in vacuum for 24 h; the products are denoted MnO_2/carbon-time (e.g., MnO_2/carbon-240).

2.2 Material and electrode characterization

X-ray diffraction patterns were recorded on a PANalytical X'Pert Pro X-ray powder diffractometer using copper $K\alpha$ radiation (λ = 1.54 Å). Nitrogen sorption isotherms were measured at 77 K with a Micromeritics ASAP 2020 analyzer. The samples were degassed in vacuum at 180 ℃ for 3 h before measurements were taken. The specific surface areas were calculated by the Brunauer–Emmett–Teller (BET) method using the adsorption branch in the relative pressure range from 0.04 to 0.25. The pore size distributions (D_P) were derived from the adsorption branch using the Barrett–Joyner–Halenda (BJH) model. Thermogravimetric analysis (TGA) was carried out in a PerkinElmer analyzer from 25 ℃ to 800 ℃ with a heating rate of 10 ℃/min and air flow rate of 100 mL/min. Scanning electron microscopy (SEM) images were obtained using a JEOL JSM-6700 FE-SEM. Transmission electron microscopy (TEM) images were obtained using a Philips CM120 microscope operated at 120 kV. High-resolution transmission electron microscopy (HRTEM) experiments were conducted on a Titan 300 kV S/TEM operated at 300 kV.

The electrodes were assembled on nickel foam collectors. Briefly, 80 wt.% of the test material, 10 wt.% of carbon black, and 10 wt.% of poly(vinylidene fluoride) dispersed in *N*-methylpyrrolidinone were mixed to form a slurry. The slurry was ultrasonically treated at 60 ℃ for 0.5 h, coated on a nickel foam substrate, and dried at 80 ℃ for 10 min under vacuum. As formed electrodes were then subjected to a pressure of 2 MPa and further dried under vacuum at 100 ℃ for 12 h. The electrochemical measurements were conducted using a Solartron 1860 electrochemistry workstation. Cyclic voltammetry measurements were conducted in 1 mol/L Na_2SO_4 aqueous solution at room temperature using a platinum wire as the counter electrode and an Ag/AgCl electrode as the reference electrode. Electrochemical impedance spectroscopy (EIS) measurements were conducted on a Solartron 1287 using a sinusoidal signal with an AC voltage of 13 mV amplitude in the frequency range from 1×10^5 to 1×10^{-2} Hz. The specific capacitance (C) of the electrode materials were derived using the equation $C = I/(\mathrm{d}E/\mathrm{d}t) \approx I/(\Delta E/\Delta t)$, where I is the constant discharge current density, E is the cell voltage, and $\mathrm{d}E/\mathrm{d}t$ is the slope of the discharge curve.

3. Results and discussion

3.1 Composition and structure of the composites

The structure and composition of the nanocomposites were found to depend strongly on the reaction conditions. Figure 1(a) compares the TGA traces of the carbon substrate and a representative composite synthesized using 0.1 mol/L $KMnO_4$ at 50 ℃ with a reaction time of 120 min (denoted as MnO_2/carbon-120). The carbon substrate lost 99.7% of its mass at 640 ℃, while the TGA curve of MnO_2/carbon-120 can be divided into three regions. The mass loss (~15%) below 200 ℃ can be ascribed to the removal of adsorbed water. It is worth mentioning that the mass loss for MnO_2/carbon-10 in this region was slightly less (~11%)

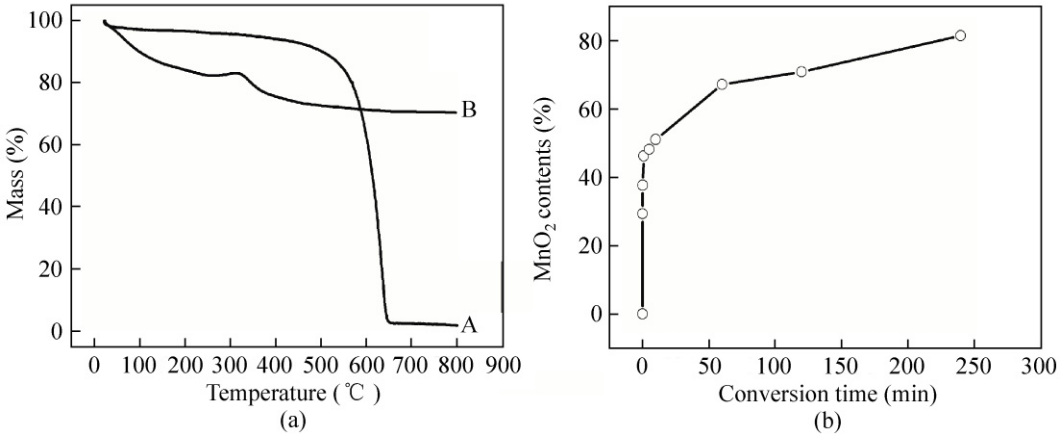

Figure 1 (a) Thermogravimetric analysis (TGA) curves of (A) the carbon substrate and (B) MnO_2/carbon-120 in air (100 mL/min). (b) Dependence of the MnO_2 content on the reaction time of the carbon substrates with $KMnO_4$ solution as measured by TGA

(Fig. S-1 in the electronic supplementary material (ESM)), which is due to its thinner MnO_2 coating that retains less interlayer hydration [40]. The mass loss between 200 ℃ and 400 ℃ corresponds to the combustion of residual carbon catalyzed by MnO_2 and its derivatives [41]. At the same time, the layered structure transformed to a thermodynamically stable tunnel structure [42, 43], and in addition δ-MnO_2 decomposed to Mn_3O_4 with release of oxygen at around 400 ℃, which also contributed to the mass loss. Above 500 ℃, residual carbon underwent combustion and Mn_3O_4 was transformed to Mn_2O_3 [44].

Based the TGA analysis, the MnO_2 contents of the composites synthesized with reaction times of 1, 5, 10, 30, 60, 120, and 240 min are compared in Fig. 1(b). It was found that the MnO_2 content increased rapidly to 46 wt.% within minutes and more slowly subsequently, due to the self-limiting growth mechanism, reaching 67 and 83 wt.% after 60 min and 240 min of the reaction, respectively. The rapid formation of MnO_2 can be attributed to the large carbon/$KMnO_4$ contact area and rapid $KMnO_4$ diffusion and reaction kinetics. Composites with 83 wt.% of MnO_2 were obtained; this is significantly higher than those prepared using mesoporous carbon or activated carbon as the sacrificed substrates (~40 wt.%) [34].

To be best of our knowledge, this content is higher than that of materials prepared using other carbon scaffolds [29, 31].

The structure of the composites was characterized using SEM, TEM, X-ray diffraction (XRD), and other techniques. Figure 2(a) shows a representative SEM image of the hierarchical carbon substrate showing the presence of macropores with diameter from 70–100 nm. Their mesoporous structure is clearly revealed under TEM observation (Fig. 2(c)). These mesoporous channels have uniform diameters in the range 6–8 nm, which is consistent with the use of F127 surfactant as the template [45]. Upon reaction with $KMnO_4$ for 120 min, the composite exhibited a rougher morphology whilst retaining the macroporous structure, and deposition of MnO_2 particles was also observed (Fig. 2(b)). TEM images (Fig. 2(d)) confirmed the retention of macropores necessary for effective electrolyte transport; the ordered carbon mesoporous texture was destroyed; however, and disordered pores are clearly present in the composite. A HRTEM image (Fig. 2(d)) suggests that the MnO_2 in the composites is polycrystalline, which is confirmed by XRD (Fig. S-2 in the ESM). The diffraction peaks in this figure marked Bir (birnessite) and Bur (buserite) are characteristic of two different types of layered δ-MnO_2 [46]: the sharp peaks occur at 2θ values of 12.5° (002) and 25° (212) can be assigned to Na-birnessite and the peak at a 2θ value of 17° to Na-buserite, with these layered structures having an interlayer separation of 0.7 Å and 1 Å, respectively [47]. The reflection marked Feit at a 2θ value of 19.1° (002) represents feitknechtite (β-MnOOH) derived from a phase transformation which depends on the MnO_4^-/Mn^{2+} ratio [48].

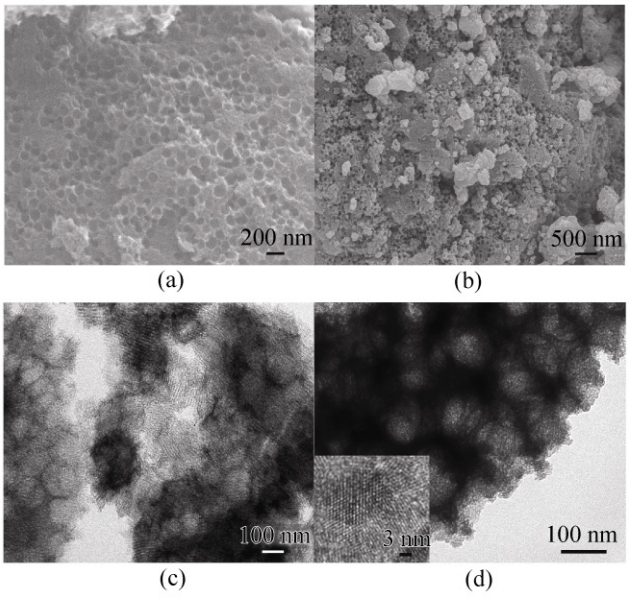

Figure 2 SEM images of (a) the carbon substrate and (b) MnO_2/carbon-120; TEM images of (c) the carbon substrate and (d) MnO_2/carbon-120 (inset, high-resolution TEM of the MnO_2 within the composite)

The pore structure of the nanocomposites was further probed using the nitrogen sorption technique. Figure 3(a) shows the nitrogen sorption isotherms and pore size distribution of the carbon substrate, clearly suggesting a hierarchical pore structure. The significant nitrogen uptake at relative pressures below 0.3 is consistent with the microporous to mesoporous structure (2–3 nm in pore diameter) created by removal of silicate clusters [49]. In addition, the isotherm curves show two substantial hysteresis loops which confirm the bimodal porosity in the meso- and macro- range, which are associated with mesoporous channels templated by the F127 surfactant and macropores templated by the silica colloids, respectively. For comparison, MnO_2/carbon-120 shows significantly different isotherms (Fig. 3(b)). The uptake at low relative pressure is significantly lower, suggesting a reduced microporosity and mesoporosity; significant uptake at high relative pressure (P/P_0) is still retained, suggesting retention of the macroporosity. In particular, the presence of the hysteresis loop concluding at a relative pressure of 0.8 indicates that the macropores are connected through a mesoporous network, forming hierarchically connected pore channels.

The above studies confirm the successful synthesis of MnO_2/carbon nanocomposites with a hierarchically porous network and tunable oxide content. The relationship between the exact location of the carbon and the oxide within the nanocomposites is unclear. Since the redox reaction was initiated from the pore surface of the carbon substrates, the rapid reaction resulted in the carbon framework becoming wrapped with a layer of MnO_2. Such a reaction may create porous nanocomposites in which the frameworks possess a "cable-like" structure made with a residual carbon core and an oxide exterior layer. Such a structure will be highly beneficial for harvesting the capacitance of the oxide; however, it is difficult to observe directly using electron microscopy and other techniques.

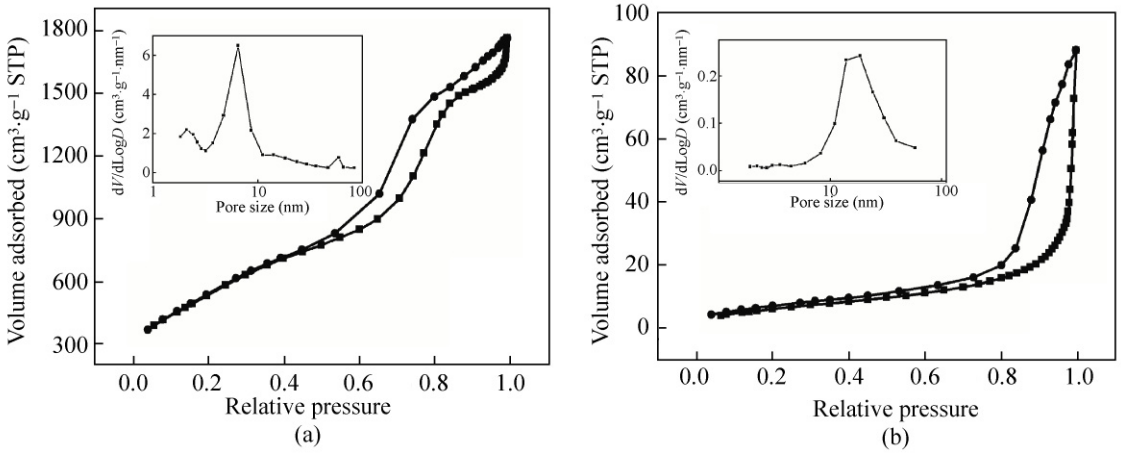

Figure 3 Nitrogen sorption isotherms and pore size distributions (insets) of (a) the hierarchical carbon substrate and (b) MnO_2/carbon-120 nanocomposite

3.2 Capacitive performance of MnO_2/carbon nanocomposites

The synthesis of MnO_2/carbon nanocomposites with a hierarchically porous network and tunable oxide content provides a unique material platform for a study of capacitance. Figure 4(a) shows the cyclic voltammetry (CV) curves of the carbon electrode. CV curves with nearly symmetrical rectangular shape were observed at potential scan rates of 5, 10, and 20 mV/s, owning to the connective pore structure and good conductivity. The MnO_2/carbon-120 electrode showed an obvious polarization, indicated by the distorted CV curve as the scan rate was increased to 20 mV/s (Fig. 4(b)). The polarization is believed to be due to the increased electron and transport resistance mentioned above. Nevertheless, with a mass loading of 70 wt.% MnO_2, the specific capacitance increased to 218 F/g at a current density of 0.1 A/g, which was three times of that of the carbon substrate (Figs. 4(c) and 4(d)).

It is well known that the capacitance generally decreases with increasing current density due to the polarization from electrolyte transport, ion diffusion or charge transfer [50, 51]. To investigate the relation between the rate capability and the oxide content, galvanostatic charge and discharge (GC) tests at various current densities were conducted (Fig. 5). Owing to the favorable pore connectivity and good conductivity, the carbon electrode retained 81% (a decrease from 71 F/g to 58 F/g) of its capacitance as the current density was increased from 0.1 to 2 A/g. After introducing the oxide with its high specific capacitance, the nanocomposites exhibited improved capacitance. For example, the MnO_2/carbon-5 electrode, with 48 wt.% MnO_2 content, gave a moderate specific

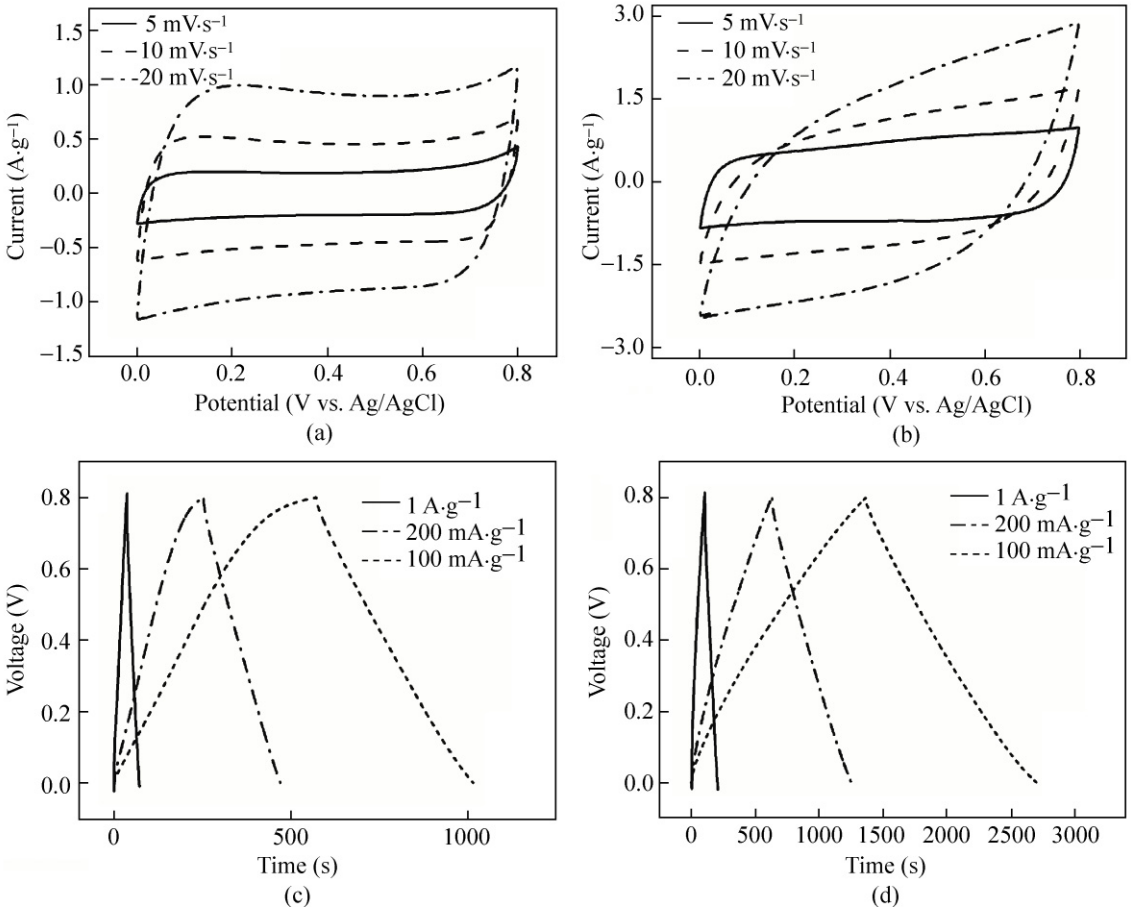

Figure 4 Cyclic voltammograms of electrodes made from (a) hierarchical carbon substrate and (b) MnO_2/carbon-120 at potential sweep rates of 5, 10, and 20 mV/s in 1 mol/L Na_2SO_4 aqueous electrolyte at room temperature; Typical charge and discharge curves of the (c) carbon and (d) MnO_2/carbon-120 electrodes at different current densities of 0.1, 0.2, and 1 A/g

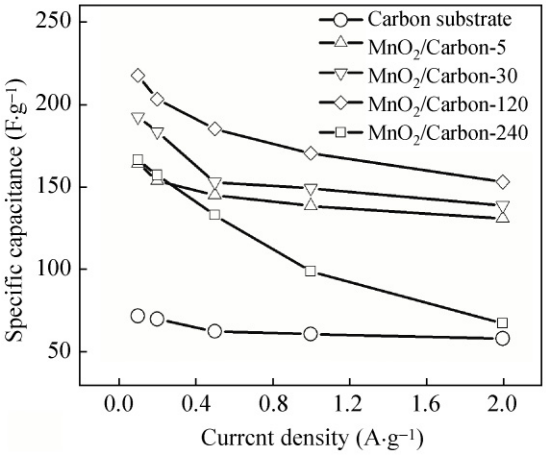

Figure 5 Gravimetric capacitance of the carbon substrate and composites with different MnO_2 content measured at charge–discharge current densities of 0.1, 0.2, 0.5, 1, and 2 A/g in 1 mol/L Na_2SO_4 aqueous electrolyte at room temperature

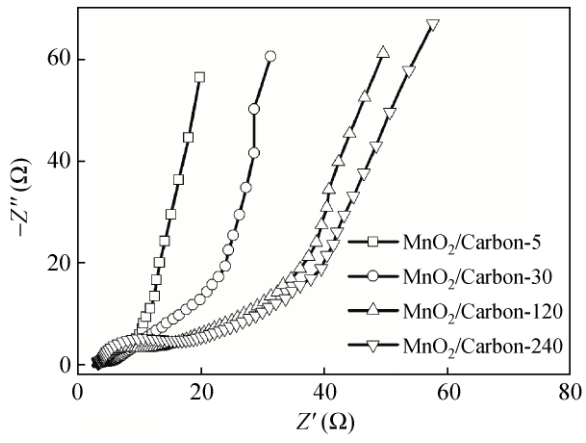

Figure 6 Nyquist plot from impedance spectroscopic analysis of the MnO_2/carbon-5 nanocomposite (□), MnO_2/carbon-30 nanocomposite (○), MnO_2/carbon-120 nanocomposite (△), and MnO_2/carbon-240 nanocomposite (▽)

capacitance of 164 F/g at a current density of 0.1 A/g; 79% capacitance was retained (130 F/g) at a current density of 2 A/g, exhibiting a good rate capability. The MnO_2/carbon-120 electrode, with 70 wt.% MnO_2 content, showed an even higher capacitance of 218 F/g at 0.1 A/g and good capacitance retention of 70% at 2 A/g. This value is about twice that of the capacitance of the MnO_2/carbon nanofoam composite prepared by a similar approach (110 F/g at 2 mV/s) [34]. However, further increasing the MnO_2 content resulted in a deterioration in the capacitance of the nanocomposites. For example, although the MnO_2/carbon-240 electrode has the highest MnO_2 loading (83 wt.%), its overall capacitance was only 166 F/g at 0.1 A/g; only 40% of its capacitance was released at a current density of 2 A/g, which is similar to that for a pure MnO_2 electrode. The deterioration in capacitance performance is due to the reduced electron conductivity (less residual carbon skeleton) and increased ion diffusion resistance (thicker MnO_2 layer).

To further understand the galvanostatic charge and discharge results, EIS was used to quantify their conductive and diffusive behavior. Figure 6 shows Nyquist plots of the composite electrodes with different oxide content, all of which have a comparable ohmic resistance. Polarization resistance (or charge transfer resistance R_P) of the electrode, shown in the high frequency region, increased gradually as the oxide content was increased. The MnO_2/carbon-240 electrode has an R_P of ~14 Ω calculated from the diameter of the semicircle, which is significantly higher than that of the MnO_2/carbon-120, MnO_2/carbon-30, and MnO_2/carbon-5 electrodes (10, 3, and 2 Ω, respectively). Assuming a bulk resistivity of MnO_2 of 5×10^5 Ω cm, a pure birnessite MnO_2 electrode with the same thickness (~20 μm) as the composite electrode will have a resistance of 1000 Ω [52]. It is clear that the carbon framework in the composites does serve as an effective conductive pathway, dramatically reducing the resistance. Note that with increasing MnO_2 content, the slope of the Nyquist plot in the low frequency region decreased gradually, indicative of the increasing Warburg resistance (or diffusion resistance). These results are in good agreement with the CV and galvanostatic charge/discharge results, verifying that higher MnO_2 content leads to larger charge transfer resistance and diffusion resistance. Therefore, to achieve good capacitance performance, it is necessary to maintain a connective carbon framework for good conductivity, and a high MnO_2 content for high specific capacitance.

Besides the improved capacitance and good rate performance, the unique composite structure creates robust oxide/carbon interfaces, which endows the nanocomposites with outstanding cycling stability. Using MnO_2/carbon-120 as an example, Fig. 7 shows the charge–discharge cycles at a constant current density of 1 A/g in 1 mol/L Na_2SO_4 electrolyte. The

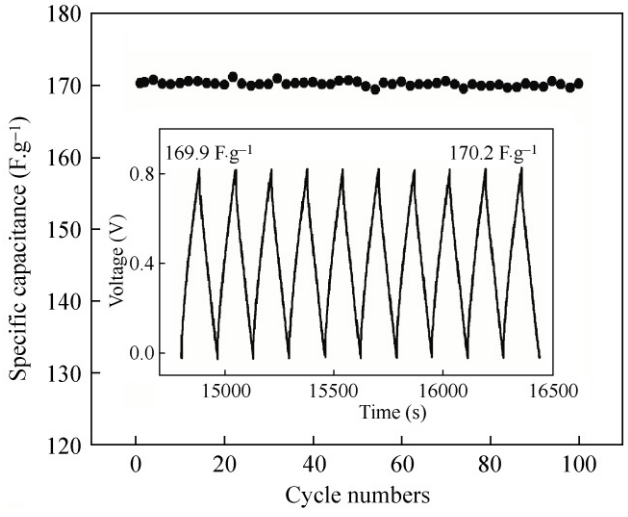

Figure 7 Cycling stability and typical charge and discharge curves (insert) of the MnO_2/carbon-120 nanocomposite at a current density of 1 A/g in 1 mol/L aqueous sodium sulfate electrolyte at room temperature

cycling performance is shown in the inset plot, which gives the GC plots from the 91st to 100th cycles. As shown, the electrode retained a very stable capacitance over 100 cycles (the capacitance decays by only 0.1%), suggesting a good electrochemical cycling stability.

4. Conclusions

We have developed a general approach to synthesize MnO_2/carbon nanocomposites with hierarchically porous structure and controllable MnO_2 loading using hierarchical carbon as the sacrificed substrate. Such unique porous substrates enable the formation of nanocomposites with high MnO_2 loading and capacitance. An EIS study suggests that increasing the MnO_2 loading also reduces the conductivity of the composites. Optimizing the MnO_2 loading and conductivity of the nanocomposites provides high specific capacitance and excellent rate capability. The fundamental understanding gained in this work will promote the design and fabrication of high-performance supercapacitors for a large variety of applications.

Acknowledgements

This work was partially supported by the Center for Molecularly Assembled Material Architectures for Solar Energy Production, Storage, and Carbon Capture, an Energy Frontier Research Center funded by the U.S. Department of Energy, Office of Science, Office of Basic Energy Sciences under award DE-SC0001342.

Electronic Supplementary Material: TGA measurements of the MnO_2/Carbon-10 nanocomposite and XRD spectra of the MnO_2/Carbon-120 nanocomposite are available in the online version of this article at http://dx.doi.org/10.1007/s12274-010-0072-y.

References

[1] Kötz, R.; Carlen, M. Principles and applications of electrochemical capacitors. *Electrochim. Acta*. **2000**, *45*, 2483–2498.

[2] Conway, B. E. *Electrochemical supercapacitors: Scientific fundamentals and technological applications*; Kluwer Academic/Plenum: New York, 1999.

[3] Huggins, R. A.; Parsons, R. Supercapacitors. *Phil. Trans. R. Soc. Lond. A*. **1996**, *354*, 1555–1566.

[4] Liu, H.; Mao, C.; Lu, J.; Wang, D. Electronic power transformer with supercapacitors storage energy system. *Electr. Pow. Syst. Res*. **2009**, *79*, 1200–1208.

[5] Raymundo-Pińero, E.; Cadek, M.; Béguin, F. Tuning carbon materials for supercapacitors by direct pyrolysis of seaweeds. *Adv. Funct. Mater*. **2009**, *19*, 1032–1039.

[6] Arico, A. S.; Bruce, P.; Scrosati, B.; Tarascon, J. M.; van Schalkwijk, W. Nanostructured materials for advanced energy conversion and storage devices. *Nat. Mater*. **2005**, *4*, 366.

[7] Chmiola, J.; Yushin, G.; Gogotsi, Y.; Portet, C.; Simon, P.; Taberna, P. L. Anomalous increase in carbon capacitance at pore sizes less than 1 nanometer. *Science* **2006**, *313*, 1760–1763.

[8] Centeno, T. A.; Stoeckli, F. On the specific double-layer capacitance of activated carbons, in relation to their structural and chemical properties. *J. Power Sources*. **2006**, *154*, 314–320.

[9] Frackowiak, E. Carbon materials for supercapacitor application. *Phys. Chem. Chem. Phys*. **2007**, *9*, 1774–1785.

[10] Zheng, J. P.; Cygan, P. J.; Jow, T. R. Hydrous ruthenium oxide as an electrode material for electrochemical capacitors. *J. Electrochem. Soc*. **1995**, *142*, 2699–2703.

[11] Subramanian, V.; Hall, S. C.; Smith, P. H.; Rambabu, B. Mesoporous anhydrous RuO_2 as a supercapacitor electrode material. *Solid State Ionics*. **2004**, *175*, 511–515.

[12] Wang, Y. G.; Wang, Z. D.; Xia, Y. Y. An asymmetric supercapacitor using RuO_2/TiO_2 nanotube composite and activated carbon electrodes. *Electrochim. Acta*. **2005**, *50*, 5641–5646.

[13] Toupin, M.; Brousse, T.; Belanger, D. Influence of microstucture on the charge storage properties of chemically synthesized manganese dioxide. *Chem. Mater*. **2002**, *14*, 3946–3952.

[14] Pang, S. C.; Anderson, M. A.; Chapman, T. W. Novel electrode materials for thin-film ultracapacitors: Comparison of electrochemical properties of sol-gel-derived and electrodeposited manganese dioxide. *J. Electrochem. Soc*. **2000**, *147*, 444–450.

[15] Chang, J.; Lee, S.; Ganesh, T.; Mane, R. S.; Min, S.; Lee, W.; Han, S. H. Viologen-assisted manganese oxide electrode for improved electrochemical supercapacitors. *J. Electroanal. Chem*. **2008**, *624*, 167–173.

[16] Subramanian, V.; Zhu, H.; Wei, B. Nanostructured MnO_2: Hydrothermal synthesis and electrochemical properties as a supercapacitor electrode material. *J. Power Sources*. **2006**, *159*, 361–364.

[17] Liu, K. C.; Anderson, M. A. Porous nickel oxide/nickel films for electrochemical capacitors. *J. Electrochem. Soc*. **1996**, *143*, 124–130.

[18] Lang, J. W.; Kong, L. B.; Wu, W. J.; Luo, Y. C.; Kang, L. Synthesis, characterization, and electrochemical properties of $Ni(OH)_2$/ultra-stable Y zeolite composite. *J. Mater. Sci*. **2009**, *44*, 4466–4471.

[19] Lin, C.; Ritter, J. A.; Popov, B. N. Characterization of sol-gel-derived cobalt oxide xerogels as electrochemical capacitors. *J. Electrochem. Soc*. **1998**, *145*, 4097–4103.

[20] Reddy, R. N.; Reddy, R. G. Porous structured vanadium oxide electrode material for electrochemical capacitors. *J. Power Sources*. **2006**, *156*, 700–704.

[21] Hu, C. C.; Huang, C. M.; Chang, K. H. Anodic deposition of porous vanadium oxide network with high power characteristics for pseudocapacitors. *J. Power Sources*. **2008**, *185*, 1594–1597.

[22] Sato, Y.; Yomogida, K.; Nanaumi, T.; Kobayakawa, K.; Ohsawa, Y.; Kawai, M. Electrochemical behavior of activated-carbon capacitor materials loaded with ruthenium oxide. *Electrochem. Solid-State Lett*. **2000**, *3*, 113–116.

[23] Kim, I. H.; Kim, J. H.; Lee, Y. H.; Kim, K. B. Synthesis and characterization of electrochemically prepared ruthenium oxide on carbon nanotube film substrate for supercapacitor applications. *J. Electrochem. Soc*. **2005**, *152*, A2170–A2178.

[24] Chen, Z.; Qin, Y.; Weng, D.; Xiao, Q.; Peng, Y.; Wang, X.; Li, H.; Wei, F.; Lu, Y. Design and synthesis of hierarchical nanowire composites for electrochemical energy storage. *Adv. Funct. Mater*. **2009**, *19*, 3420–3426.

[25] Wu, M.; Snook, G. A.; Chen, G. Z.; Fray, D. Redox deposition of manganese oxide on graphite for supercapacitors. *J. Electrochem. Commun*. **2004**, *6*, 499–504.

[26] Huang, X.; Yue, H.; Attia, A.; Yang, Y. Preparation and properties of manganese oxide/carbon composites by reduction of potassium permanganate with acetylene black. *J. Electrochem. Soc*. **2007**, *154*, A26.

[27] Ma, S. B.; Lee, Y. H.; Ahn, K. Y.; Kim, C. M.; Oh, K. H.; Kim, K. B. Spontaneously deposited manganese oxide on acetylene black in an aqueous potassium permanganate solution. *J. Electrochem. Soc*. **2006**, *153*, C27–C32.

[28] Zhu, S.; Zhou, H.; Hibino, M.; Honma, I.; Ichihara, M. Synthesis of MnO_2 nanoparticles confined in ordered mesoporous carbon using a sonochemical method. *Adv. Funct. Mater*. **2005**, *15*, 381–386.

[29] Dong, X.; Shen, W.; Gu, J.; Xiong, L.; Zhu, Y.; Li, H.; Shi, H. J. MnO_2-embedded-in-mesoporous-carbon-wall structure for use as electrochemical capacitors. *J. Phys. Chem. B*. **2006**, *110*, 6015–6019.

[30] Zhang, H.; Cao, G.; Wang, Z.; Yang, Y.; Shi, Z.; Gu, Z. Growth of manganese oxide nanoflowers on vertically-aligned carbon nanotube arrays for high-rate electrochemical capacitive energy storage. *Nano Lett*. **2008**, *8*, 2664–2668.

[31] Raymundo-Piñero, E.; Khomenko, V.; Frackowiak, E.; Béguin, F. Performance of manganese oxide/CNTs composites as electrode materials for electrochemical capacitors. *J. Electrochem. Soc*. **2005**, *152*, A229–A235.

[32] Lee, C. Y.; Tsai, H. M.; Chuang, H. J.; Li, S. Y.; Lin, P.; Tsen, T. Y. Characteristics and electrochemical performance of supercapacitors with manganese oxide-carbon nanotube nanocomposite electrodes. *J. Electrochem. Soc*. **2005**, *152*, A716–A720.

[33] Fan, Z.; Chen, J.; Wang, M.; Cui, K.; Zhou, H.; Kuang, Y. Preparation and characterization of manganese oxide/CNT composites as supercapacitive materials. *Diam. Relat. Mater*. **2006**, *15*, 1478–1483.

[34] Fischer, A. E.; Pettigrew, K. A.; Rolison, D. R.; Stroud, R. M.; Long, J. W. Incorporation of homogeneous, nanoscale MnO_2 within ultraporous carbon structures via self-limiting electroless deposition: Implications for electrochemical capacitors. *Nano Lett*. **2007**, *7*, 281–286.

[35] Chu, H. Y.; Lai, Q. Y.; Wang, L.; Lu, J. F.; Zhao, Y. Preparation of MnO_2/WMNT composite and MnO_2/AB composite by redox deposition method and its comparative study as supercapacitive materials. *Ionics*. **2009**, *16*, 233–238.

[36] Wang, D. W.; Li, F.; Liu, M.; Lu, G.; Cheng, H. M. 3D aperiodic hierarchical porous graphitic carbon material for high-rate electrochemical capacitive energy storage. *Angew. Chem. Int. Ed*. **2008**, *47*, 373–376.

[37] Jiao, F.; Bruce, P. G. Mesoporous crystalline β-MnO_2-reversible positive electrode for rechargeable lithium batteries. *Adv. Mater*. **2007**, *5*, 657–660.

[38] Jin, X.; Zhou, Wu.; Zhang, S.; Chen, G. Z. Nanoscale microelectrochemical cells on carbon nanotubes. *Small*. **2007**, *3*, 1513–1517.

[39] Meng, Y.; Gu, D.; Zhang, F.; Shi, Y.; Yang, H.; Li, Z.; Yu, C.; Tu, B.; Zhao, D. Ordered mesoporous polymers and homologous carbon frameworks: Amphiphilic surfactant templating and direct transformation. *Angew. Chem. Int. Ed.* **2005**, *44*, 7053–7059.

[40] Feng, Q.; Sun, E. H.; Yanagisawa, K.; Yamasaki, N. Synthesis of birnessite-type sodium manganese oxides by solution reaction and hydrothermal methods. *J. Ceram. Soc. Jpn*. **1997**, *105*, 564–568.

[41] Shen, B.; Qin, L. Study on MSW catalytic combustion by TGA. *Energy Convers. Manage*. **2006**, *47*, 1429–1437.

[42] Liu, L.; Feng, Q.; Yanagisawa, K.; Wang, Y. Characterization of birnessite-type sodium manganese oxides prepared by hydrothermal reaction process. *J. Mater. Sci. Lett*. **2000**, *19*, 2047–2050.

[43] Feng, Q.; Yanagisawa, K.; Yamasaki, N. Synthesis of birnessite-type potassium manganese oxide. *J. Mater. Sci. Lett*. **1997**, *16*, 110–112.

[44] Sharma, R. K.; Oh, H. S.; Shul, Y. G.; Kim, H. Growth and characterization of carbon-supported MnO_2 nanorods for supercapacitor electrode. *Phy. Rev. B: Condens. Matter*. **2008**, *403*, 1763–1769.

[45] Liu, R.; Shi, Y.; Wan, Y.; Meng, Y.; Zhang, F.; Gu, D.; Chen, Z.; Tu, B.; Zhao, D. Triconstituent co-assembly to ordered mesostructured polymer−silica and carbon−silica nanocomposites and large-pore mesoporous carbons with high surface areas. *J. Am. Chem. Soc*. **2006**, *128*, 11652–11662.

[46] Vol'khin, V. V.; Pogodina, O. A.; Leont'eva, G. V. Nonstoichiometric compounds based on manganese(III, IV) oxides with the birnessite structure. *Russ. J. Gen. Chem*. **2002**, *72*, 173–177.

[47] Devaraj, S.; Munichandraiah, N. Effect of crystallographic structure of MnO_2 on its electrochemical capacitance properties. *J. Phys. Chem. C*. **2008**, *112*, 4406–4417.

[48] Luo, J.; Huang, A.; Park, S. H.; Suib, S. L.; O'Young, C. Crystallization of sodium β-birnessite and accompanied phase transformation. *Chem. Mater*. **1998**, *10*, 1561–1568.

[49] Hu, Q.; Lu, Y.; Meisner, G. P. Preparation of nanoporous carbon particles and their cryogenic hydrogen storage capacities. *J. Phys. Chem. C*. **2008**, *112*, 1516–1523.

[50] Brock, S. L.; Duan, N.; Tian, Z. R.; Giraldo, O.; Zhou, H.; Suib, S. L. A review of porous manganese oxide materials. *Chem. Mater*. **1998**, *10*, 2619–2628.

[51] Toupin, M.; Brousse, T.; Belanger, D. Charge storage mechanism of MnO_2 electrode used in aqueous electrochemical capacitor. *Chem. Mater*. **2004**, *16*, 3184–3190.

[52] Guzman, R. N. D.; Awaluddin, A.; Shen, Y.; Tian, Z.; Suib, S. L.; Ching, S.; O'Young, C. Electrical resistivity measurements on manganese oxides with layer and tunnel structures: Birnessites, todorokites, and cryptomelanes. *Chem. Mater*. **1995**, *7*, 1286–1292.